applied sciences

MDPI

Article

A Software-Defined Radio Platform for Teaching Beamforming Principles

Annamaria Sârbu [1,*], Robert Papa [2], Angela Digulescu [3,4] and Cornel Ioana [4,5]

[1] Department of Telecommunication, Information Technology and Cyber Security, "Nicolae Bălcescu" Land Forces Academy Sibiu, 550170 Sibiu, Romania
[2] Faculty of Electronics, Telecommunications and Information Technology, Technical University of Cluj Napoca, 400114 Cluj-Napoca, Romania; papa.robert02@yahoo.com
[3] Department of Telecommunications and Information Technology, Military Technical Academy "Ferdinand I", 050141 București, Romania; angela.digulescu@mta.ro
[4] Altrans Energies, 38031 Grenoble, France; cornel.ioana@altransinnov.com
[5] GIPSA-LAB, Universite Grenoble-Alpes, 38400 Saint-Martin-d'Hères, France
* Correspondence: paljanosanna@yahoo.com

Featured Application: This paper presents the design, validation, and testing of a software-defined radio beamforming platform designed for educational purposes.

Abstract: This paper presents the development and validation of a hybrid beamforming system based on software-defined radio (SDR), designed for telecommunications engineering education. The system provides an agile and user-friendly platform that allows students to observe, test, and evaluate beamforming techniques in real time. The platform integrates a multichannel SDR device (USRP N310) with traditional radiofrequency equipment and open-source software, facilitating hands-on learning experiences. The paper details the proposed hardware and software architecture and documents the calibration and validation phases. The testing and validation processes were conducted using a 3.5 GHz antenna array in both indoor and outdoor environments. The results demonstrated the system's effectiveness in achieving the desired beam orientations, with experimental results aligning closely with simulation and theoretical predictions. Significant differences in the radiation patterns observed between the indoor and outdoor measurements were documented, highlighting the impact of environmental factors on beamforming performance. The insights gained from this research provide valuable contributions to the education of future telecommunications engineers, enhancing their understanding of practical beamforming applications and the integration of modern SDR technology.

Keywords: software-defined radio (SDR); beamforming; telecommunication education; phase calibration

Citation: Sârbu, A.; Papa, R.; Digulescu, A.; Ioana, C. A Software-Defined Radio Platform for Teaching Beamforming Principles. *Appl. Sci.* **2024**, *14*, 10386. https://doi.org/10.3390/app142210386

Academic Editor: Alessandro Lo Schiavo

Received: 24 October 2024
Revised: 7 November 2024
Accepted: 8 November 2024
Published: 12 November 2024

1. Introduction

Beamforming has emerged as an essential technology in today's wireless communication landscape, enabling more efficient, reliable, and high-speed data transmission in fifth-generation mobile communication (5G) and wireless-fidelity (Wi-Fi) networks by focusing signals to end-user devices. This is achieved through signal processing techniques that steer the beam in specific directions by combining outputs from multiple antennas or arrays.

As the demand for bandwidth and connectivity continues to increase, beamforming plays a crucial role in optimizing signal directivity, by minimizing interference and enhancing overall performance in both indoor and outdoor wireless communication environments [1]. In indoor environments, where radio waves must propagate through walls, furniture, and other obstructions, beamforming dynamically directs signals towards the end-user receivers, reducing the effects of multipath propagation and attenuation. In outdoor environments, wave propagation is impacted by factors such as longer

transmission distances, diverse weather conditions, and the presence of buildings and foliage [2]. By directing radio beams towards user devices, beamforming aims to compensate signal fading and scattering, common propagation phenomena in outdoor environments. Figure 1 presents 5G and Wi-Fi beamforming networks deployed in indoor and outdoor environments.

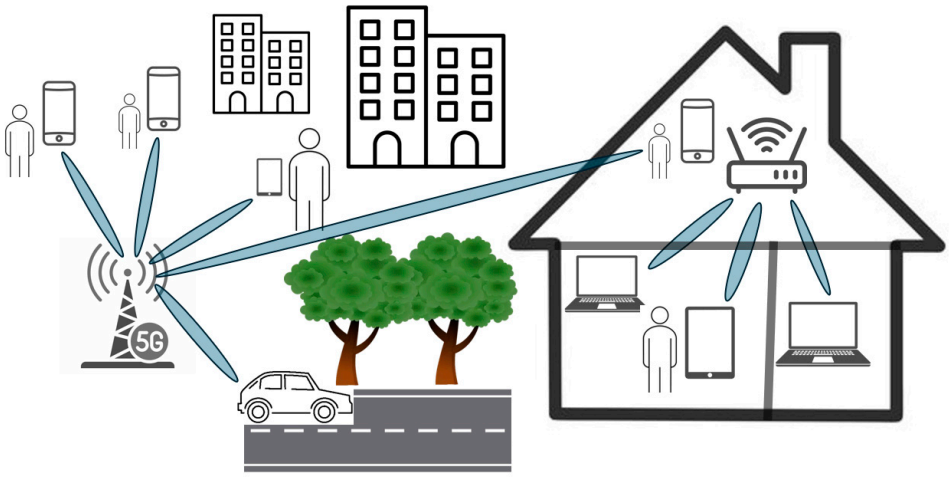

Figure 1. 5G and Wi-Fi beamforming networks deployed in indoor and outdoor environments.

Beamforming can be implemented using analog, digital, or hybrid architectures [3–7], each with its own advantages and limitations. Analog beamforming is more cost-effective as it uses fewer radiofrequency (RF) chains [4], but it is limited in flexibility due to its inability to independently control the signal on each antenna element. On the other hand, digital beamforming has been proved to be highly flexible and convenient for implementing complex algorithms as it relies on software-based signal processing [5]. However, this comes at a higher cost and greater complexity compared to analog beamforming. Hybrid beamforming, which combines analog and digital components, can significantly reduce hardware complexity and power consumption while approaching the performance of fully digital beamforming [3,6].

Hybrid beamforming is a promising approach offering a balance between performance and hardware efficiency [6,7]. Coupled with the agility and flexibility of software-defined radio (SDR) technology, this approach enables convenient, rapid, and cost-effective deployment of communication systems in multiple frequency bands [8,9]. To this extent, several papers document the use of SDR for beamforming systems [8–11]. The authors of [8] demonstrate that their proposed SDR-based beamforming system effectively cancels interference in multipath environments without compromising signal quality or performance. In [9], the authors present a flexible SDR-based radio beamforming architecture operating in the 28 GHz frequency band with potential application in radar and 5G systems. SDR-based beamforming systems are also presented in [10–13], with demonstrated usability and robustness together with good agreement between simulation and measurement results. The main documented challenge associated with the use of SDR for beamforming is the need of phase calibration in the case of multiple transmitters for precise beam directivity [14]. Despite these advancements, gaps and limitations still exist in the current literature, particularly concerning the documentation of phase synchronization, as well as the validation and testing of these systems in real-life deployment scenarios in the sub 6 GHz frequency range [15], where propagation impact is more significant than in mm-wave.

Multichannel transmit/receive SDR recently became available from NI Ettus Research [16] or Per Vices Corporation [17], supporting a variety of RF developing environments. Building on this accessibility, this work presents the development of an SDR-based beamforming platform designed for laboratory experimentation of telecom engineering students. The proposed system is based on hybrid architecture, allowing students to ex-

plore and implement beamforming techniques on customizable antenna platforms. By providing this hands-on experience with real-world wireless communication, the students can delve into a deeper understanding of modern RF and signal processing concepts.

The contributions of this work include the development and validation of a hybrid SDR-based beamforming system aimed at providing telecom engineering students with an agile, user friendly, educational platform for observing, testing, and evaluating beamforming. This paper also documents the identified challenges associated with the use of an SDR for beamforming along with testing and validation on an array of patch antennas operating in the 3.5 GHz frequency band. The beamforming platform was deployed in both indoor and outdoor environments in order to observe the differences in the system behavior in both environments.

The remainder of the paper is structured into four sections, with Section 2 detailing the system hardware and software architecture. Section 3 describes the system parametrization, while Section 4 is focused on the implementation and testing of the beamforming system on a custom-designed antenna. The final section presents the conclusions of the paper.

2. System Architecture

The beamforming platform was designed to combine commercial of-the-shelf RF products, which are typically accessible in any telecommunication laboratory. The aim of this approach is to develop students' competencies in integrating SDR, traditional RF equipment, and open software, offering them hands-on experience in using the customized beamforming platform.

2.1. Hardware Architecture

The central element of the beamforming system is the USRP N310 device [18], a multichannel SDR device featuring four transmit (TX) and four receive channels, operating in the frequency range of 10 MHz–6 GHz. The hardware architecture of the USRP N310 is based on two RF daughterboards, each with a dedicated local oscillator (LO). An external LO followed by an RF splitter was used to achieve phase synchronization on all four transmit channels, as N310 does not support LO sharing between the two daughterboards (a feature that was fixed in the USRP X serries [19]). The Anapico APSIN20G RF frequency generator [20] was used to generate an LO frequency twice the frequency of the desired RF output ($f_{LO} = 2 \times F_{TX}$) with an amplitude of +5 dBm, ensuring that the amplitude after the RF splitter remains between 0 and 6 dBm [18]. The antenna under test (AUT) can be composed of individual monopole antenna elements like those used in Wi-Fi routers or a 1×4 array of patch antenna. Each of the USRP TX channels can be physically connected to the AUT ports either by direct SMA RF connection or equal-length RF cables to ensure phase stability among the antenna elements.

A small dimension Aaronia PBS1 electric field probe [21] with a sensor diameter of 3 mm was connected to one RX channel of the USRP device. The E field probe is used to measure the amplitude received over the air (OTA) at different azimuthal points in a semicircle. The distance between the AUT and the receiving E field probe could be varied between 20 cm and 6 m, depending on the length of the RF cable used for connecting the E field probe to the USRP RX channel. The measurement distance should be chosen to meet the far-field criteria ($2D^2/\lambda$), calculated according to the operating frequency/wavelength (λ) and the device under test dimension (D). Thus, given the minimum operating frequency of 300 MHz, 6 m should be considered sufficient to meet the far-field criteria for a device under test with a maximum dimension of 3 m. A computer running Ubuntu with GNU Radio 3.10.7 open-source software [22] was used to control the USRP. Figure 2 presents the diagram of the proposed system architecture.

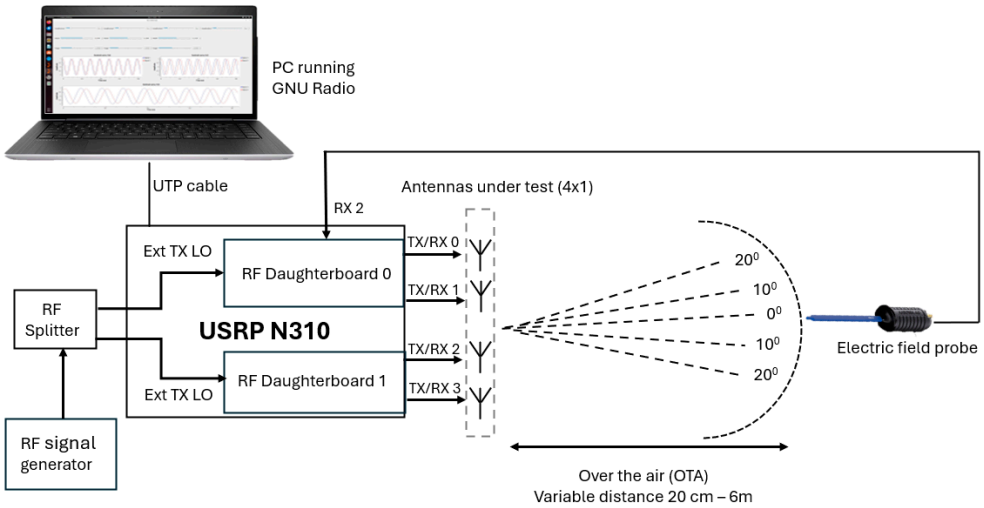

Figure 2. Beamforming platform architecture.

The designed platform supports experimental flexibility, as it can be used on any beamforming device with up to four radiating elements operating in the frequency range of 300 MHz to 4000 MHz. The platform enables variation of the antenna element type, size, or spacing to include intuitive experiments on array beam direction and sidelobe variations. The frequency range limitation for the USRP N310 device is given by the acceptable LO inputs [18]. More advanced SDR hardware can be used to increase the frequency range or the number of TX channels. To this extent, USRP X410 supports direct LO sharing between the RF motherboards, resulting in an increased frequency range (1 MHz up to 7.2 GHz), and USRP X440 can be used to increase the number of channels up to eight. The Cyan SDR manufactured by Per Vices [17] can support up to 16 combinations of RX and TX channels in the near DC to 18 GHz frequency range. As SDR hardware platforms continue to evolve, they are expected to support even higher frequency ranges, including millimeter-wave applications in the 5G/6G FR2 bands, which extend up to 40 GHz.

2.2. Software Interface

A customized user interface was designed in GNU Radio for setting the individual phases and amplitudes of the four USRP RF channels used for transmission (TX). The GNU Radio flowchart used for transmission is depicted in Figure 3.

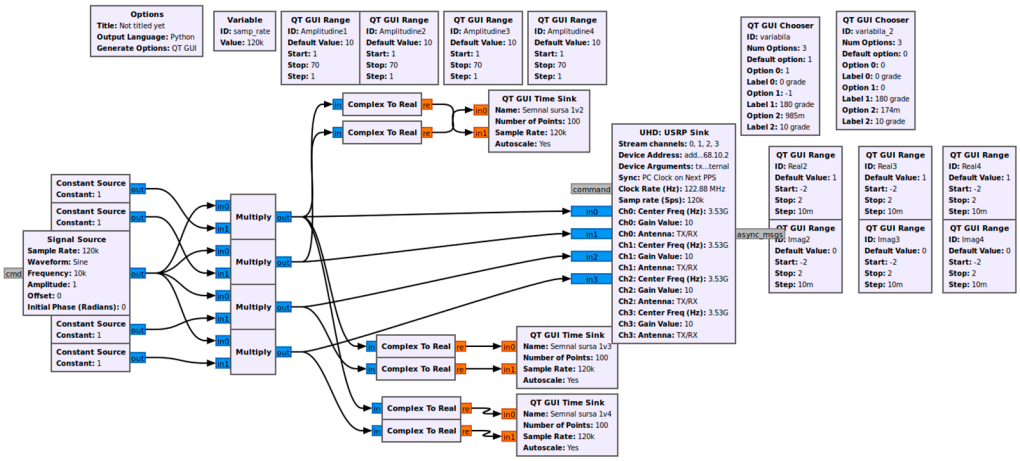

Figure 3. GNU Radio transmission flowchart.

For the TX system, we have set up a single sinusoidal signal source block that generates a signal s[n] according to Equation (1).

$$s[n] = A \times [\cos(2\pi \frac{f}{fs} n) + j \times \sin(2\pi \frac{f}{fs} n)] \quad (1)$$

where A is the signal amplitude set in the block's parameters, f is frequency of the baseband sine wave (set to 10 kHz), and fs is the sampling rate (set to 120 kHz). The output of the signal source block was split in four (each for one TX channel) and passed to a multiplication block. The multiplication block multiplies the signal with a complex constant, resulting in signals $s_i[n]$, with i ranging from one to four, corresponding to each of the TX channels. The expression of the signal $s_i[n]$ is calculated according to Equation (2).

$$s_i[n] = (Real_i + jImag_i) \times A \times [\cos(2\pi \frac{f}{fs} n) + j \times \sin(2\pi \frac{f}{fs} n)] \quad (2)$$

The values of the real ($Real_i$) and imaginary ($Imag_i$) parts of the multiplication constants can be modified for TX channels 2–4 using QT GUI Range type variables. According to Equation (2), the phase of the signals on each of the TX channels is thus modified by setting the complex value of the constant source block. By modifying the phase of the signal on each of the TX channels, the beam can be steered in real time towards the desired azimuthal location, observing the principle of beamforming.

Three QT GUI Time Sink blocks were configured to view the waveforms of signals $s_i[n]$, $i \in [2,4]$, versus $s_1[n]$, with the phase difference between the channels referenced to the phase of the signal corresponding to TX channel 1. The digital-to-analog converter converts the $s_i[n]$ IQ digital signal to the analog signal $s_i(t)$, where it mixes it with the LO frequency (f_{LO}) to obtain the RF signal $s_{TX}(t)$. In the USRP Sink block, we have configured four TX channels. The center frequency parameter of the USRP Sink block sets the RF frequency of the TX channel and is set in this example to 3.53 GHz.

The amplitude of each individual channel can be modified by setting the value of the gain parameter in the USRP Sink block, also configured by a QT GUI type variable. The user interface obtained after running the GNU Radio flowchart is presented in Figure 4, enabling real-time setting of amplitude and phase for USRP TX channels 1–4.

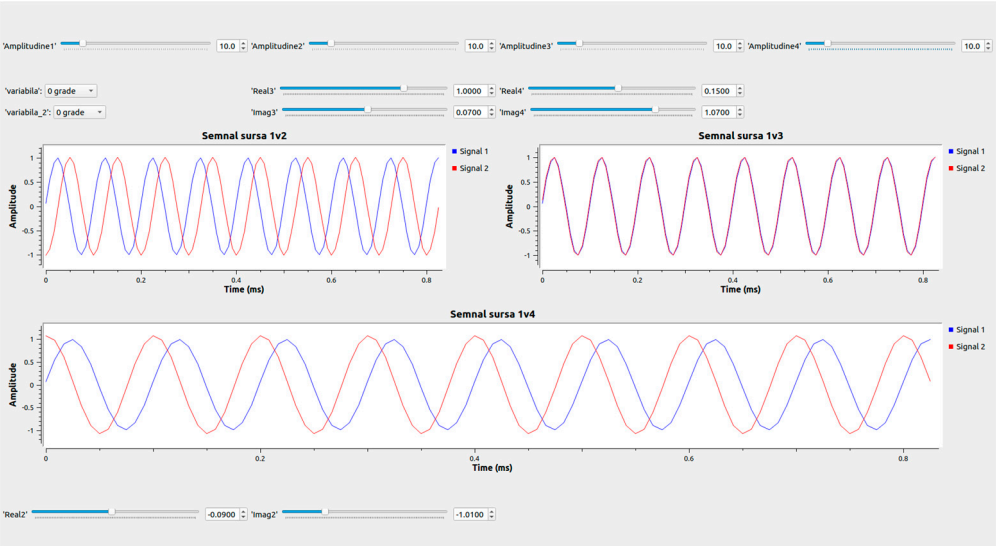

Figure 4. GNU Radio interface for setting TX channel phase/amplitude.

The RX channel is also configured within GNU Radio, according to the flowchart presented in Figure 5 (top), by setting a USRP source on the center frequency of 3.53 GHz and using a QT GUI Frequency Sink type block. The lower part of Figure 5 presents

the corresponding frequency spectrum, with the measured 3.53 GHz continuous signal. With the E field probe connected to the USRP RX channel and the flowchart running, the variation in the amplitude received can be observed in real−time.

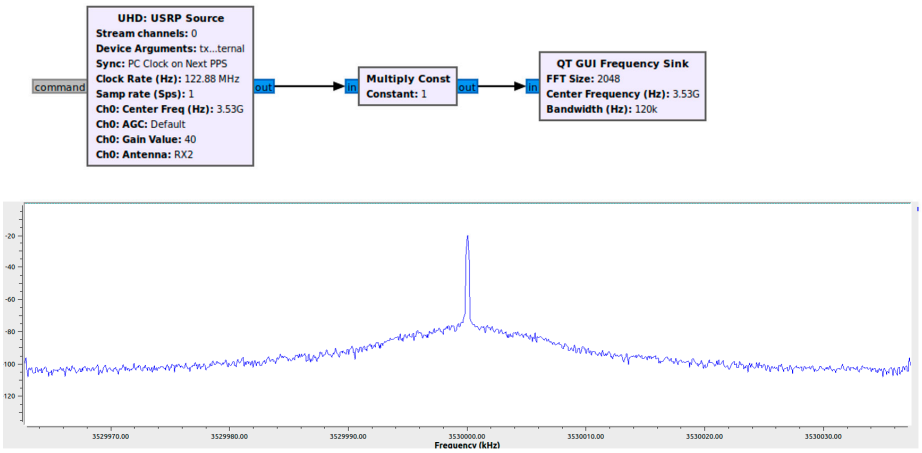

Figure 5. GNU Radio flowchart (**top**) and spectrum (**bottom**) for TX channel.

3. System Parametrization

In beamforming systems, or any other system that requires synchronized transmission across multiple channels, accurate phase and amplitude calibration for all channels is crucial for ensuring optimal performance. Unlike traditional RF equipment such as spectrum analyzers (SAs) or oscilloscopes, SDRs are not factory-calibrated in terms of phase and amplitude response. Their versatility and flexibility come at the cost of requiring careful calibration to ensure that the system performs as intended. Without calibration, SDR devices can introduce errors that impact the precision and coherence of the signals. Parametrization ensures that the phase and amplitude corrections are not static but adaptive, meaning they can change depending on the deployed hardware or software architecture (cable type, frequency range, and GNU Radio parameter settings).

This section details the parametrization caried out for deploying the beamforming system on a 1×4 array of patch antennas in the 3.53 GHz frequency range. Both phase and amplitude parametrizations were carried out for the four TX channels and the RX channel. One must note that any change in hardware or software implementation could require a new parametrization.

The phase variation was validated using an Rhode&Schwartz(R&S) RTO2064 oscilloscope featuring four channels (CH), 6 GHz bandwidth, and 20 GSa/s maximum sample rate. The four TX channels of the URSP were connected by RF cables (same type and length) to each of the four oscilloscope channels. Figure 6 presents a picture of the experimental setup used for phase alignment of the four USRP TX channels, with one group of channels (CH1 and 3) being set out of phase compared to the other group of channels (CH2 and 4).

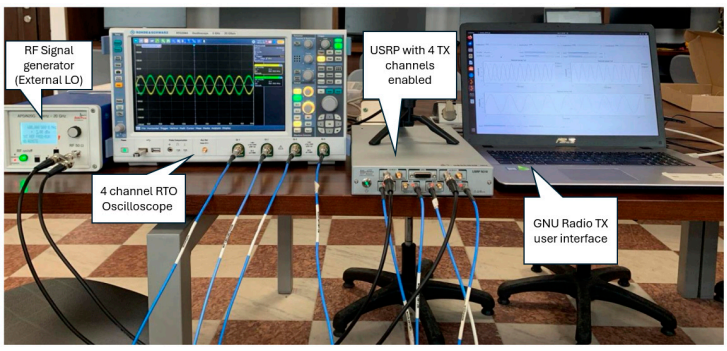

Figure 6. Experimental setup for phase alignment.

Figure 7 presents the result of the phase calibration for 3.53 GHz frequency after the values of the complex constants were set to correspond to 0° phase difference between the four TX channels. The signal waveforms were displayed as time domain diagrams and as an XY type diagram. In the XY type diagram the signal on the X axis was set to channel 1 and the signal on the Y axis to channels 2, 3, and 4, respectively.

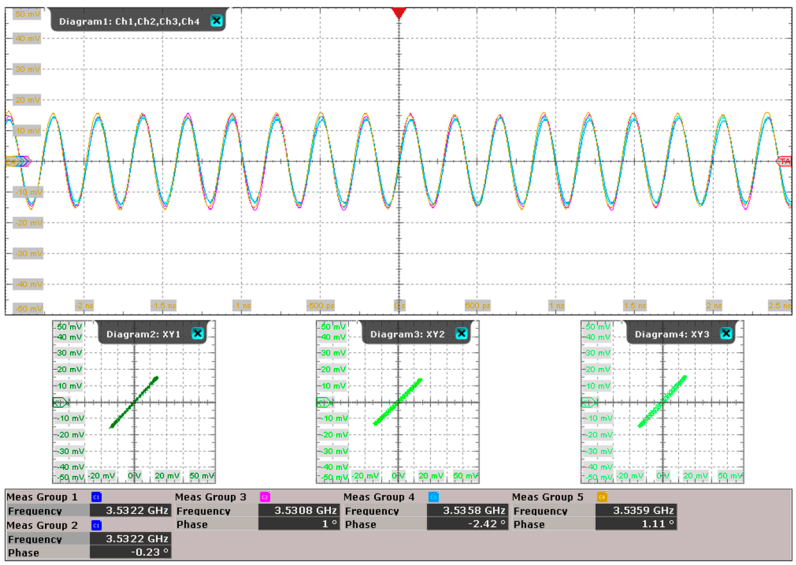

Figure 7. Phase alignment measurement for 3.53 GHz TX frequency.

The system maintains the phase calibration each time it is powered on if the operating frequency and hardware (splitter and cables) remains unchanged. Calibration is required for each operating frequency and was observed to persist over multiple experiments and device functioning hours. To ensure proper system functioning, a new calibration needs to be performed each time the frequency of the system is changed.

The time–amplitude view in Figure 6 (top) reveals that the four TX USRP channels perfectly overlap, while the XY diagrams show very good alignment between CH1 and CH2/CH3. In the second XY diagram (bottom middle), one can observe that the phase alignment between CH1 and CH3 is not optimal, with a maximum measured phase offset of 2.4°. This deviation was attributed to the instrument limitations given by factors such as the frequency stability of the LO, noise, component tolerances, and even small physical damage of hardware. However, as will be demonstrated in the following subsection, the slight phase misalignment did not significantly impact the overall performance of the system that was intended for demonstration and learning purposes.

The amplitude calibration of the TX channels was performed with an R&S FSV3013 SA. Figure 8a presents an example of the measured 3.53 GHz frequency signal for a gain value of 20 dB (TX1), with the visible SA settings and TX channel directly connected by RF cable. Figure 8b presents the amplitude linearity measured for one of the USRP TX channels.

It was observed that all channels demonstrated similar variation in amplitude linearity, so in Figure 8b, we present the result of a single TX channel amplitude linearity measurement. One can note the good amplitude linearity of the USRP TX channel. Even if the TX gain (dB) does not directly correspond to the measured SA power in dBm, good linear agreement between the two variables was discovered.

For calibrating the USRP RX channel, a continuous wave signal was generated with a signal generator and measured alternatively using the USRP RX interface and the SA. Figure 9a presents the experimental setup used for USRP RX channel parametrization. The multiplication constant in Figure 5 was modified to achieve agreement between the SA and USRP measured power values, as presented in Figure 9b.

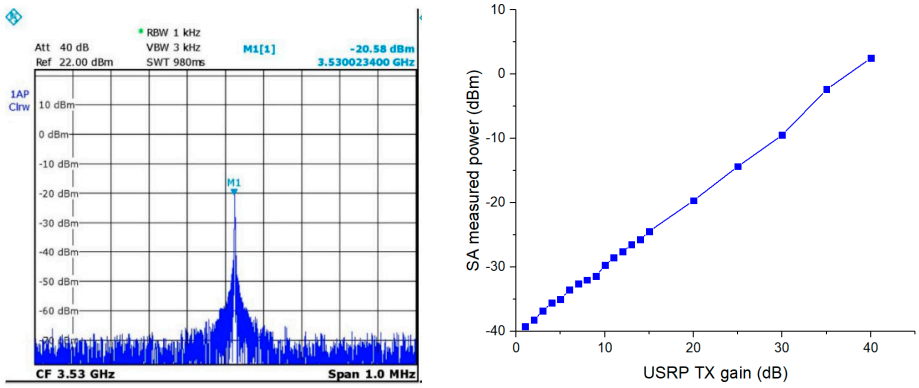

Figure 8. (**a**) SA measurement of USRP TX signal amplitude; (**b**) USRP TX channel amplitude linearity.

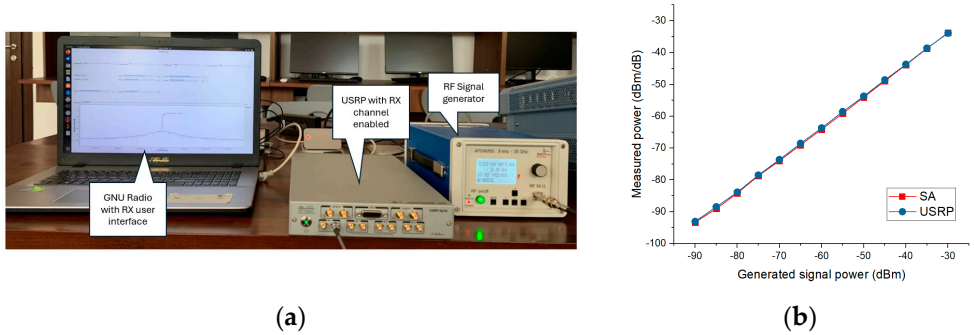

Figure 9. (**a**) Experimental setup for RX parametrization; (**b**) USRP/SA RX amplitude linearity.

4. Beamforming Platform Validation and Testing

The beamforming platform validation and testing were conducted using a customized array of patch antennas, with experimental measurements performed in both indoor and outdoor environments. The system was tested for different beam orientations by applying phase shifts between the patch elements and measuring the resulting radiation patterns.

4.1. Design and Characterization of an Array of Patch Antennas

A customized 1 × 4 array of patch antennas was designed in CST Studio Suite to operate in the 3.5 GHz frequency range, emulating a device operating in the 5G FR1. The dimensions of each patch were set at 28 mm wide and 19 mm high, with a distance of 4.42 mm between each patch. To ensure proper feeding, each patch element was connected through a feeder with a width of 2.8 mm and a height of 8.32 mm, values calculated to obtain a characteristic impedance of 50 Ohms on each antenna port. In addition, to facilitate practical handling, an additional copper-free substrate element has been added to the bottom of the antenna to create a solid handle.

Through the optimization process, adjustments were made to the patch dimensions, increasing the width by 0.138 mm and the height by 0.469023 mm. These modifications were implemented to correct the deviations identified in the simulation results and achieve optimized antenna parameters. The antenna was then printed on an FR4 substrate. Figure 10 presents the configuration of the designed (a) and manufactured (b) antenna.

Figure 11 presents the array of patch antennas' 3D radiation pattern(a) as well as the horizontal 2D radiation pattern (b), extracted from simulation for 0° phase offset between the patch elements. One can observe the forward direction of the main radiation lobe with the presence of two smaller sidelobes.

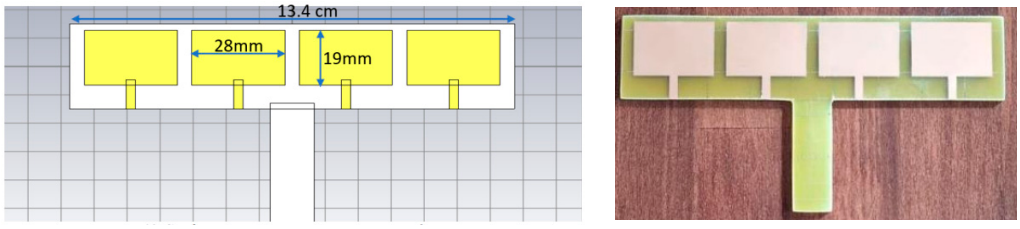

(**a**) (**b**)

Figure 10. (**a**) Designed patch antenna; (**b**) physical patch antenna.

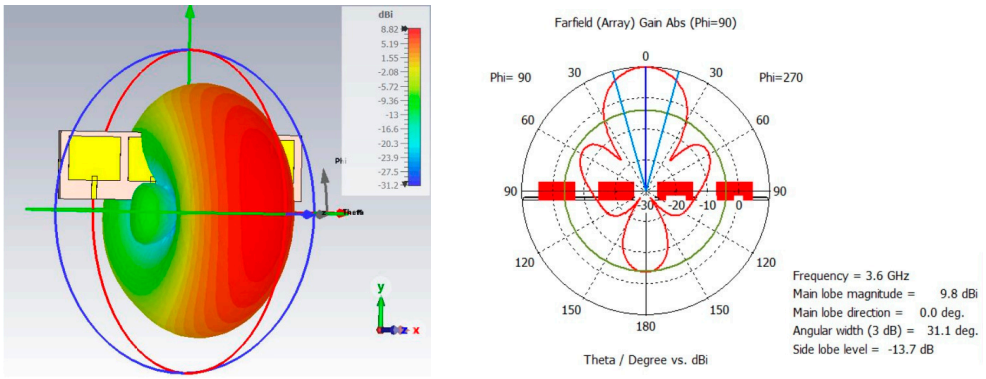

(**a**) (**b**)

Figure 11. Array of patch antennas' radiation pattern in (**a**) 3D and (**b**) azimuth.

By modifying the phase of the signal fed to each patch element, the user can shift the beam towards the desired azimuthal direction. From phased array antenna theory [23], the azimuthal orientation or the steering angle of the beam (θ), relative to the forward direction, can be calculated based on the wavelength (λ), the element spacing (d), and the phase shift per element (ΔΦ) based on Equation (3). A schematic representation of the beamforming process for the designed patch antenna is presented in Figure 12.

$$\theta = \arcsin\left(\frac{\lambda \Delta\phi}{2\pi d}\right) \quad (3)$$

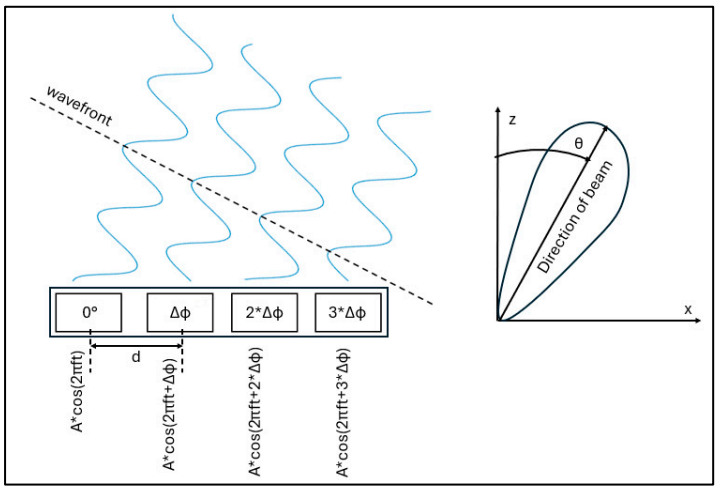

Figure 12. Phased array beamformer principle.

To validate the physical antenna, the scattering (S) parameters of the patch antenna were measured using a two-port R&S ZNB Vector Network Analyzer (VNA) and compared to the simulation results. Measurements were performed indoors, in a laboratory.

The S_{11} parameter in Figure 13a corresponds to a single patch element (the first), while S_{12} was measured between patch element 1 and 2. In the simulation, the antenna resonant frequency was 3.6 GHz, and the associated S_{11} value was −12 dB, while measurements indicated an actual resonant frequency at 3.53 GHz, with a measured S_{11} parameter of −8.5 dB. The observed 70 MHz shift in the resonant frequency (from 3.6 GHz to 3.53 GHz) is relatively small (around 2%). However, the S_{11} discrepancy indicates that the antenna reflects more power than expected, suggesting either increased losses or a mismatch between the antenna and its feed.

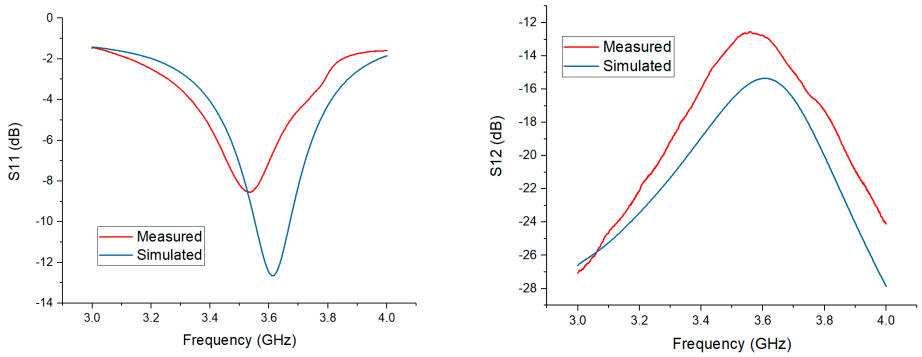

(**a**) (**b**)

Figure 13. Measured and simulated S11 (**a**) and S12 (**b**) parameters.

The discrepancies between simulated and measured values can be attributed to several factors, including fabrication tolerances, material properties, environmental factors, and model assumptions. Variations in the manufacturing process, such as slight changes in the dimensions of the antenna or the dielectric properties of the substrate (real versus simulated) can lead to the observed differences. One must also consider the presence of interference and reflections in the laboratory environment during measurements due to the presence of walls, furniture, and objects, which were not modeled in the CST Studio Suite simulation.

The factors detailed above also explain the differences observed for the coupling between the patch antenna elements, as quantified by the S_{12} parameter (Figure 13b). The coupling effect of consecutive patch elements was observed to be most significant for consecutive patch elements, as the case of S12 presented, and less significant for patch elements spaced further.

Even though the antenna efficiency is not ideal, one must keep in mind that the antenna is intended for short-distance transmission, so authors appreciate that this design will be sufficient for the assumed objective. Further antenna optimization is possible but does not constitute the main effort of this paper as it is important to balance design efforts with real-world needs.

4.2. Beamforming Platform Testing in Indoor and Outdoor Environments

The functioning of the beamforming system was experimentally verified both indoors (in a laboratory) and outdoors (open area) by performing measurements of the patch antenna radiated pattern in an azimuthal plane. The experimental setup used for indoor measurement of the radiation pattern is present in Figure 14, with a similar setting being deployed outdoors in an open area of 2400 m^2. While controlled measurements in an anechoic chamber were not possible due to resource limitations, this approach was considered suitable for the defined objective, as will be further demonstrated. Due to the close positioning of the measuring probe and the antenna, we can assume that the measured field value is attributed to the antenna under test, allowing for sufficient data collection to understand the basic behavior of beamforming. Additionally, the use of both indoor and

outdoor settings gives students a more comprehensive understanding of how beamforming performs under different environmental conditions.

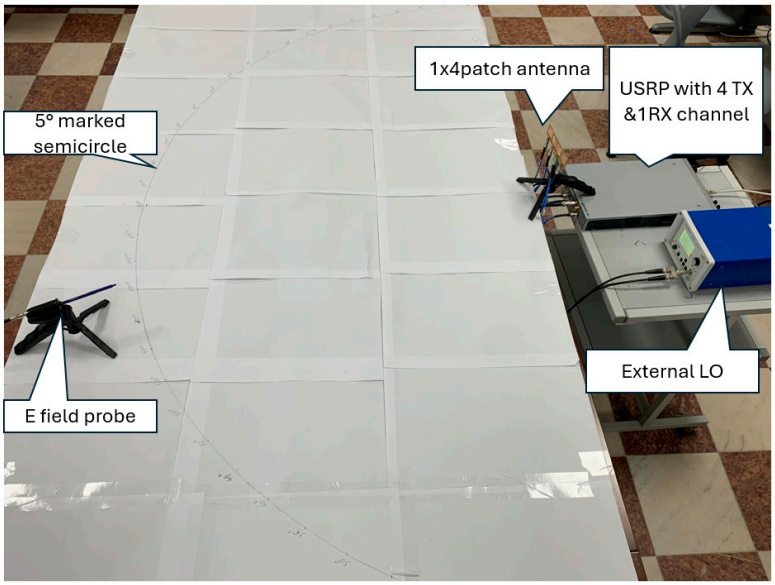

Figure 14. Experimental setup for indoor radiation pattern measurement.

For the indoor scenario, the radiation pattern was measured in a 60 m^2 laboratory, for one horizontal plane placed at 90 cm above floor level, in a semicircle with a spatial resolution of 5°. The patch antenna was connected by RF cables (same type and equal length) to the four TX channels of the USRP. An Aaronia PBSE field probe connected to the USRP RX channel was used for measuring signal strength. The field values were recorded for each azimuthal orientation in a semicircle with a radius of 1 m, considered suitable for the used frequency of 3.53 GHz (λ = 8.49 cm). Two beam orientations were measured: 1. No phase offset between the patch elements (phase values of 0°/0°/0°/0°). 2. A phase difference of 45° between consecutive patch elements (0°/45°/90°/135°). According to Equation (3), the beam steering resulting from the second phase difference would be approximately 20° for the designed patch antenna. Based on Equation (3), and the maximum measured phase variation of 2.42°, we have calculated a maximum error in the steering angle deviation of 1.01°, which is considered suitable given manual positioning of the E field probe and the spatial resolution of the measurement.

The designed graphical user interface presented in Section 2.2 was used to apply the values of the TX channels phase differences.

Figure 15 presents the results of the measured radiation patterns in both indoor/outdoor scenarios for two beam orientations: forward −90° and 20° tilt −right. The plotted data were interpolated by a factor of five using a spline function to achieve a better resolution (1°).

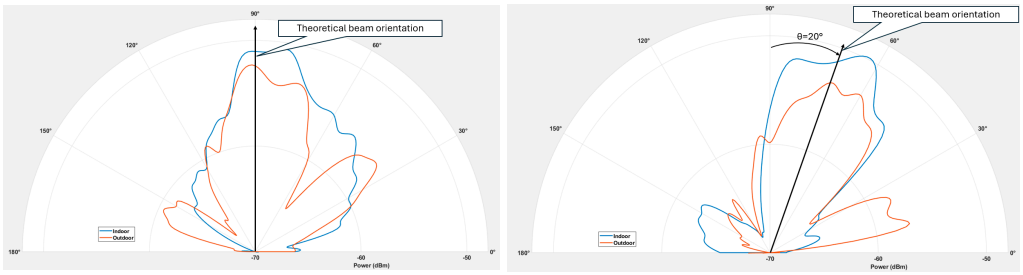

Figure 15. Indoor/outdoor measured radiation pattern for two beam orientations.

First, there is a notable difference in the beam patterns obtained in indoor and outdoor environments. In an indoor environment, there are more reflections and diffraction effects due to walls, furniture, and other obstacles. The multipath propagation occurring in an indoor environment typically results in a more complex or distorted beam pattern compared to outdoor environment. This explains why the small antenna side lobes are not visible for indoor measurements but become visible when the beamforming system is deployed outdoors. We can also observe that path loss is generally lower indoors due to the confined space but tends to fluctuate more due to reflections.

Outdoor measurements revealed that the 90° beam orientation was in good agreement with the simulation results, as presented by Figure 11. For the 20° tilt beam orientation, we can once again observe the presence of the two sidelobes in the outdoor measurement results, while only one sidelobe is visible in the indoor setting. Also, for the second beam orientation, one can observe good agreement with the analytically derived solution, supporting a 20° beam steer compared to the no-phase-difference scenario. These observations validate the beamforming platform's effectiveness in achieving the desired beam orientation while demonstrating the influence of environmental factors on the radiation pattern.

5. Conclusions

In this paper, we present the development, calibration, validation, and testing of a hybrid beamforming system aimed at providing telecommunication engineering students with an interactive, user-friendly platform for observing and testing beamforming principles. By integrating a commercial multichannel SDR device with traditional RF equipment and open-source software, the proposed platform contributes to the development of students' practical abilities and a deeper understanding of signal-processing techniques in real-world applications.

Along with its main objective, this paper also documents the challenges associated with using an SDR platform for beamforming, emphasizing the need for accurate phase and amplitude calibration and parametrization to ensure optimal system performance in beamforming applications.

The system is tested on a customized 1×4 patch antenna, designed to operate in the 3.53 GHz frequency range. The system validation was achieved through experimental measurements, with results demonstrating the main differences in the behavior of a beamforming system in indoor and outdoor environments. The reported results also validate the effectiveness of the beamforming platform in achieving the desired steering angles, with good agreement between experimental and simulated/analytical results.

The use of the proposed platform will engage students in the fundamental principles of telecommunication and will trigger the development of essential professional competencies. By exploiting the versatility of SDR devices, they could enable, observe, and test various beamforming technologies, preparing them for the future challenges in telecommunication engineering.

We have thus demonstrated that utilizing open-source hardware for system experimentation in telecommunication education is feasible and beneficial for promoting cost-effective educational initiatives. The proposed SDR platform, paired with open-source software and affordable hardware components, can effectively support hands-on learning experiences. This setup not only allows students to experiment with real-time beamforming but also provides a flexible, scalable system adaptable to a range of experimental configurations and frequencies.

Author Contributions: Conceptualization, A.S. and C.I.; data curation, R.P. and C.I.; formal analysis, A.D.; funding acquisition, C.I.; investigation, A.S. and R.P.; methodology, A.S.; project administration, C.I.; resources, A.D. and C.I.; software, R.P.; supervision, A.S. and A.D.; writing—original draft, A.S.; writing—review and editing, A.S. and A.D. All authors have read and agreed to the published version of the manuscript.

Funding: This research received no external funding.

Institutional Review Board Statement: Not applicable.

Informed Consent Statement: Not applicable.

Data Availability Statement: The original contributions presented in this study are included in the article. Further inquiries can be directed to the corresponding author.

Acknowledgments: This work has been funded in part by the R&I program of ALTRANS Energies.

Conflicts of Interest: The authors declare no conflict of interest.

References

1. Mismar, F.; Evans, B.; Alkhateeb, A. Deep Reinforcement Learning for 5G Networks: Joint Beamforming, Power Control, and Interference Coordination. *IEEE Trans. Commun.* **2019**, *68*, 1581–1592. [CrossRef]
2. Azevedo, J.A.; Mendonça, F. A Critical Review of the Propagation Models Employed in LoRa Systems. *Sensors* **2024**, *24*, 3877. [CrossRef] [PubMed]
3. Sohrabi, F.; Yu, W. Hybrid Digital and Analog Beamforming Design for Large-Scale Antenna Arrays. *IEEE J. Sel. Top. Signal Process.* **2016**, *10*, 501–513. [CrossRef]
4. Ratnam, V.; Molisch, A. Periodic Analog Channel Estimation Aided Beamforming for Massive MIMO Systems. *IEEE Trans. Wirel. Commun.* **2019**, *18*, 1581–1594. [CrossRef]
5. Spoof, K.; Tenhunen, M.; Unnikrishnan, V.; Stadius, K.; Kosunen, M.; Ryynänen, J. True-Time-Delay Receiver IC With Reconfigurable Analog and Digital Beamforming. *IEEE Access* **2022**, *10*, 116375–116383. [CrossRef]
6. Hamid, S.; Chopra, S.R.; Gupta, A.; Tanwar, S.; Florea, B.C.; Taralunga, D.D.; Alfarraj, O.; Shehata, A.M. Hybrid Beamforming in Massive MIMO for Next-Generation Communication Technology. *Sensors* **2023**, *23*, 7294. [CrossRef] [PubMed]
7. Gadiel, G.M.; Lee, K. Energy-Efficient Hybrid Beamforming with Variable and Constant Phase Shifters. *Appl. Sci.* **2019**, *9*, 4476. [CrossRef]
8. Gaydos, D.; Nayeri, P.; Haupt, R. Adaptive Beamforming With Software-Defined-Radio Arrays. *IEEE Access* **2022**, *10*, 11669–11678. [CrossRef]
9. Marinho, D.; Arruela, R.; Varum, T.; Matos, J. Software-Defined Radio Beamforming System for 5G/Radar Applications. *Appl. Sci.* **2020**, *10*, 7187. [CrossRef]
10. Wang, J.; Mouthaan, K. Robust Beamforming for Conformal Antenna Arrays using Software Defined Radio. In Proceedings of the 2021 IEEE International Symposium on Antennas and Propagation and USNC-URSI Radio Science Meeting (APS/URSI), Singapore, 4–10 December 2021; pp. 1485–1486. [CrossRef]
11. Wang, J.; Mouthaan, K. LCMV Beamforming for Conformal Arrays Using Software Defined Radio. In Proceedings of the 2020 International Symposium on Antennas and Propagation (ISAP), Osaka, Japan, 25–28 January 2021; pp. 795–796. [CrossRef]
12. Jean, M.; Yuksel, M.; Gong, X. Millimeter-Wave Software-Defined Radio Testbed with Programmable Directionality. In Proceedings of the IEEE INFOCOM 2023—IEEE Conference on Computer Communications Workshops (INFOCOM WKSHPS), Hoboken, NJ, USA, 20 May 2023; pp. 1–8. [CrossRef]
13. Nayeri, P.; Haupt, R.L. A testbed for adaptive beamforming with software defined radio arrays. In Proceedings of the 2016 IEEE/ACES International Conference on Wireless Information Technology and Systems (ICWITS) and Applied Computational Electromagnetics (ACES), Honolulu, HI, USA, 13–18 March 2016; pp. 1–2. [CrossRef]
14. Dusari, N.; Rawat, M. Phase Calibration of Multiple Software Defined Radio Transmitters for Beamforming in 5G Communication. In Proceedings of the 2021 National Conference on Communications (NCC), Kanpur, India, 27–30 July 2021; pp. 1–5. [CrossRef]
15. Demeneghi, J.A.; Kaur, J.; Tan, K.; Abbas, H. Sub-6 GHz beamforming with low-cost software-defined radio: Design, testing, and performance evaluation. *Phys. Commun.* **2024**, *65*, 102391. [CrossRef]
16. Available online: https://www.ettus.com/product-categories/usrp-networked-series/ (accessed on 4 October 2024).
17. Available online: https://www.pervices.com/cyan/ (accessed on 4 October 2024).
18. Available online: https://kb.ettus.com/N300/N310 (accessed on 7 October 2024).
19. Available online: https://www.ettus.com/product-categories/usrp-x-series/ (accessed on 7 October 2024).
20. Available online: https://www.testequipmenthq.com/datasheets/ANAPICO-APSIN20G-Datasheet.pdf (accessed on 7 October 2024).
21. Available online: https://downloads.aaronia.com/datasheets/antennas/Probes/Aaronia_Probe_Set.pdf (accessed on 7 October 2024).
22. Perotoni, M.; Santos, K. SDR-Based Spectrum Analyzer Based in Open-Source GNU Radio. *J. Microw. Optoelectron. Electromagn. Appl.* **2021**, *20*, 542–555. [CrossRef]
23. Jackson, D. Phased Array Antenna Handbook (Third Edition) [Book Review]. *IEEE Antennas Propag. Mag.* **2018**, *60*, 124–128. [CrossRef]